processes

MDPI

Article

Competitive Adsorption of Pb^{2+} from Aqueous Solutions by Multi-Source Lignocellulose-Derived Hydrothermal Humic Acid

Changzhi Song [1], Junhao Liu [2], Libo Zhang [3,4,*], Jianing Wang [3] and Xinqian Shu [1]

[1] School of Chemistry and Environmental Engineering, China University of Mining and Technology Beijing, Beijing 100083, China; changzhi.song@uq.net.au (C.S.); sxq@cumtb.edu.cn (X.S.)
[2] School of Environment, Tsinghua University, Beijing 100084, China; junhaoliu25@outlook.com
[3] Guangdong Provincial Engineering and Technology Center for Corrosion and Safety in Petrochemical Industry, School of Chemical Engineering, Guangdong University of Petrochemical Technology, Maoming 525000, China; wangjianing62022@163.com
[4] State Key Laboratory of Heavy Oil Processing, College of Engineering, China University of Petroleum-Beijing at Karamay, Karamay 834000, China
* Correspondence: zhanglibo@cupk.edu.cn

Abstract: This study explores the conversion of lignocellulosic biomass from softwood, hardwood, and grasses into humic acid via a mild hydrothermal process and its application in Pb^{2+} adsorption. The investigation focused on adsorption isotherms, kinetics, thermodynamics, and the intraparticle diffusion model to evaluate the adsorption performance of humic acids from different sources. The results indicate that the humic acid of broad-leaved wood (Eucalyptus-HA) possesses the optimal adsorption capacity and removal efficiency of Pb^{2+}. When the initial concentration of Pb^{2+} is 100 mg/L, the adsorption capacity and removal efficiency of Eucalyptus-HA reach 49.75 mg/g and 25.57%, respectively, which are far higher than the adsorption capacity (26.82 mg/g) and removal efficiency (13.71%) of commercial humic acid (Commercial-HA). The pore structure of humic acid plays a critical role in its Pb^{2+} adsorption capacity. High Pb^{2+} concentrations and a low pH negatively impact adsorption efficiency, and instability in the humic acid pore structure affects reproducibility. Adsorption isotherm fitting showed that Pb^{2+} adsorption conforms most closely to the Langmuir model. While commercial humic acid exhibited faster adsorption rates, its capacity was constrained by thermodynamic limitations and lower specific surface areas. The intraparticle diffusion model revealed that Pb^{2+} diffusion proceeded more efficiently in hydrothermal humic acids than in commercial ones due to lower diffusion resistance. This study highlights the potential of feedstock source regulation to enhance humic acid's heavy metal adsorption capabilities, expanding its application across various fields.

Keywords: lignocellulosic biomass; hydrothermal conversion; humic acid; Pb^{2+} adsorption; kinetics; thermodynamics; internal diffusion model

check for updates

Academic Editor: Maria Victoria López Ramón

Received: 12 December 2024
Revised: 26 December 2024
Accepted: 30 December 2024
Published: 8 January 2025

Citation: Song, C.; Liu, J.; Zhang, L.; Wang, J.; Shu, X. Competitive Adsorption of Pb^{2+} from Aqueous Solutions by Multi-Source Lignocellulose-Derived Hydrothermal Humic Acid. *Processes* **2025**, *13*, 155. https://doi.org/10.3390/pr13010155

Copyright: © 2025 by the authors. Licensee MDPI, Basel, Switzerland. This article is an open access article distributed under the terms and conditions of the Creative Commons Attribution (CC BY) license (https://creativecommons.org/licenses/by/4.0/).

1. Introduction

Humic acid is derived from organic matter, like plant residues, through microbial processes. The molecular structure diagram of humic acid is shown in Figure 1. It stands out as a noteworthy example of natural material transformation, constituting over half of the organic matter in soils and playing a crucial role in soil fertility [1]. This substance is rich in functional groups such as carboxyl, hydroxyl, and methoxy groups, which aid in promoting crop growth by stimulating seed germination and enhancing early seedling emergence. Additionally, humic acid boosts root vitality and improves the ability of plant roots to absorb nutrients and water, functioning as a versatile organic soil fertilizer [2].

Its multifunctional characteristics also allow it to complex with heavy metals, making it useful in environmental remediation, especially in the adsorption of organic pollutants [3]. Currently, humic acid is produced extensively using two primary methods: extraction from lignite and peat, or the composting of organic materials such as agricultural and forestry waste, sludge, and livestock manure [4]. The first method is hindered by the non-renewable nature of its raw materials, while the second encounters difficulties in managing the composition and structure of humic acid due to the environmental sensitivities of the composting process. Consequently, chemical methods present a promising alternative; they not only speed up traditional fermentation but also allow for the control of various parameters during chemical reactions, facilitating the optimized adjustment of humic acid's structure and composition for a wider range of applications.

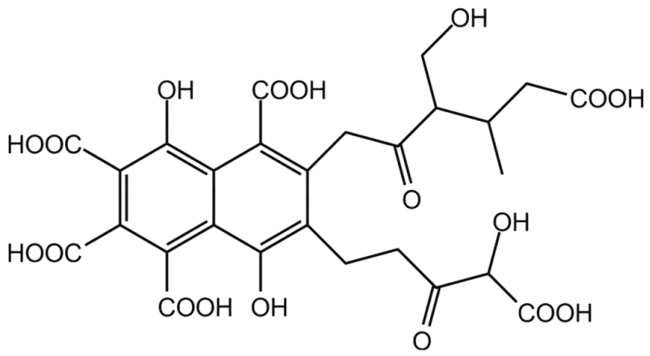


Figure 1. Humic acid molecular structure diagram.

The application of mild hydrothermal conversion to turn agricultural and forestry waste biomass into humic acid has shown considerable promise for practical use. Yang et al. utilized hydrothermal reactions to mimic geochemical processes, using kitchen waste as their raw material for synthesizing humic acid. In comparison to humic acid extracted from soil, the humic acid obtained from kitchen waste exhibited a lower molecular weight and a higher oxygen content, indicating that hydrothermal conversion can effectively influence the composition and properties of humic acid [5]. Similarly, Chen et al. used food waste as their feedstock and obtained humic acid through a reaction at 215 °C for 1 h. Their characterization results showed that the produced humic acid had a structure and composition similar to that of humic acid extracted from minerals. Moreover, the proteins in food waste, through reactions between sugars and amino acids, significantly promoted the formation of humic acid [6]. However, overall research on humic acid formation via hydrothermal processes remains in its early stages.

In previous studies conducted by our research group, various types of lignocellulosic biomass (softwood, hardwood, grasses, and model biomass components) were utilized to produce humic acid under optimized hydrothermal conditions (200 °C, 4 h, 0.5 M NaOH). Among these, fir wood powder yielded the highest humic acid output (29.82 wt %). One of these studies systematically examined the influence of operational parameters and feedstock properties on humic acid production from lignocellulosic biomass, revealing a strong correlation between humic acid yield and the lignin content of the biomass [7]. However, specific application scenarios and the performance of humic acids derived from different sources were not investigated, which poses challenges for subsequent modifications and performance enhancements.

With industrial development, large quantities of lead-containing waste are being discharged into the environment, severely contaminating water and soil. Lead primarily exists in the form of Pb(II), which can bioaccumulate through the food chain and enter the human body, affecting neurological and renal functions. Current remediation techniques for

Pb^{2+}-contaminated water and soil include chemical precipitation, electrolysis, ion exchange, bioremediation, and adsorption. Among these, adsorption is widely applied due to its simplicity and low cost. There have also been studies using humic acid as an adsorbent for Pb^{2+} removal. For instance, Dai et al. extracted humic acid from sludge, and its loose, clustered structure, along with its abundant oxygen-containing functional groups, enabled efficient Pb^{2+} adsorption (27.59 mg/g) [8]. Zhao et al. prepared artificial humic acid from food waste through biological fermentation, using it to simultaneously remove lead(II) and cadmium(II) from water. Their study found that electrostatic interactions, complexation, ion exchange, and adsorption were the primary mechanisms influencing the removal efficiency of heavy metals by humic acid [9].

However, there is a notable lack of comparative studies on the properties of feed-stock materials in the field of humic acid-based heavy metal adsorption, as well as insufficient analysis from the perspectives of adsorption kinetics and thermodynamics. Such information is crucial for the targeted regulation of humic acid.

In light of this, the present study first synthesized and compared humic acids from different sources (fir powder representing softwood, eucalyptus powder representing hardwood, rice straw representing grasses, and commercial humic acid) using a hydrothermal method. The adsorption performance of these humic acids in removing lead ions (Pb^{2+}) was evaluated, and a structural characterization of the humic acids was conducted to analyze the structural factors influencing adsorption efficiency. The optimal lignocellulosic humic acid for Pb^{2+} adsorption was identified. Next, the humic acid with the best Pb^{2+} adsorption performance was selected for a systematic comparison with commercial humic acid in terms of lead ion adsorption efficiency, including adsorption processes and mechanisms. Detailed thermodynamic and kinetic comparisons were carried out, aiming to provide a reference for the targeted regulation of humic acid structure and composition for different application scenarios.

2. Materials and Methods

2.1. Materials

Samples of Metasequoia and eucalyptus wood powders were sourced from a furniture factory in Beijing, China, while rice straw powder was collected from farmland in Jiangsu Province, China. The raw lignocellulosic materials were washed with water, dried at 105 °C until a constant weight was achieved, and then ground to a 200-mesh size for further use. Sodium hydroxide (NaOH), hydrochloric acid (HCl), and nitric acid (HNO_3) (all of analytical grade), along with microcrystalline cellulose ($(C_6H_{10}O_5)_n$), xylan ($(C_5H_8O_4)_n$), sodium lignosulfonate ($C_{20}H_{24}Na_2O_{10}S_2$), and commercial humic acid (obtained through alkaline extraction from inferior lignite that was fully carbonized, with a fulvic acid content exceeding 90%), were obtained from Sigma-Aldrich. The deionized water (18.25 MΩ·cm) used in the experiments was prepared in-house using a water purification system (WP-UP-UV-20, Sichuan Water Technology Development Co., Ltd., Chengdu, China).

2.2. Preparation of Hydrothermal Humic Acid from Lignocellulosic Biomass from Different Sources

Following the previously established experimental protocol [10], a specific amount of lignocellulosic biomass was weighed and immersed in a 0.5 M NaOH solution. The reaction took place at 200 °C for 4 h in a six-position parallel high-pressure reactor (Guizhou Shanli Experimental Instruments Co., Ltd., Guiyang, China). Following the reaction, the reactor was promptly cooled to room temperature utilizing an ice-water bath. Subsequently, the reactor valve was opened to release the gas products, and the resulting liquid–solid mixture was filtered under vacuum through a Büchner funnel. To guarantee the complete transfer of the product, the reactor was rinsed with 0.5 M NaOH. The filtrate was then acidified

with 1 M HCl to adjust its pH to a range of 2–3, causing the solid products to precipitate out. These solids were harvested by centrifugation at 8000 rpm for 10 min and subsequently dried at a temperature of 105 °C.

The hydrothermal humic acids derived from fir powder, eucalyptus wood powder, and rice straw powder were labeled as Abies fabri-HA, Eucalyptus-HA, and Rice straw-HA, respectively, while the commercial humic acid was designated Commercial-HA.

2.3. Characterization of Humic Acid

Point of zero charge (PZC) measurement: The point of zero charge (PZC) of the humic acids was measured according to the referenced method [9]. The PZC of the various humic acid samples was measured using the pH drift method on a Zeta potential analyzer (90 Plus, Brookhaven, GA, USA).

2.4. Adsorption of Pb^{2+} by Humic Acid

2.4.1. Humic Acid Adsorption of Pb^{2+} Test

According to the method described in the reference [9], a 0.01 M sodium nitrate solution was first prepared and used to dissolve a lead acetate solution at a specific concentration. A certain mass of humic acid was weighed and placed into a prepared lead acetate solution. Under a specific temperature, magnetic stirring was applied to create a vortex. After a certain period of adsorption, the humic acid was separated using a high-speed centrifuge, and the resulting liquid was the lead ion solution after adsorption (note that the time is counted from 0 min when the humic acid is initially added). The volume of the post-adsorption lead acetate solution, V_1 (mL), was measured, and the concentration of Pb^{2+} ions was determined using the EDTA titration method. The adsorption experiments of Pb^{2+} onto humic acid at different pH values were conducted by adjusting the pH of the sodium nitrate and lead acetate mixture to the desired levels using 0.1 M HNO_3.

2.4.2. Determination of Pb^{2+} Concentration

Following the titration method described in the reference [11], a 3.2×10^{-6} mol/L hydrochloric acid solution (pH = 5.5) was prepared and used to make a 0.2 g/L Na_2-EDTA solution as the titrant. A 2 g/L solution of xylenol orange was prepared as the indicator. The pH of the lead nitrate solution obtained in Section 2.4.1 was adjusted to approximately 5.5 using 0.25 M NaOH. Under stirring conditions, the Na_2-EDTA solution was titrated into the lead nitrate solution at pH 5.5. The titration endpoint was reached when the solution color changed from purple-red to yellow-orange. The volume of Na_2-EDTA consumed, V_2 (mL), was recorded. The Pb^{2+} concentration at a given time point could then be calculated using the following equation:

$$C_t(g/L) = V_2 \times 0.2 \times 207.2/(336.24 \times V_1) \quad (1)$$

$$Q_t\left(\frac{mg}{g}\right) = \frac{V(C_0 - C_t)}{m} \quad (2)$$

$$R\ (\%) = \frac{C_0 - C_t}{C_0} \times 100 \quad (3)$$

where V is the volume of lead nitrate solution to be adsorbed, C_0 is the initial concentration of Pb^{2+}, and C_t is the equilibrium concentration of Pb^{2+} at time t.

3. Results and Discussion

3.1. Comparison of Lead Ion Adsorption Properties of Humic Acids from Different Sources

Coniferous wood, represented by Abise fabri; broad-leaved wood, represented by eucalyptus; grass biomass, represented by rice straw; and commercial humic acid were purchased, and the differences in the adsorption capacity Q_t of Pb^{2+} and the removal rate R of the humic acid from these different sources are shown in Figure 2.

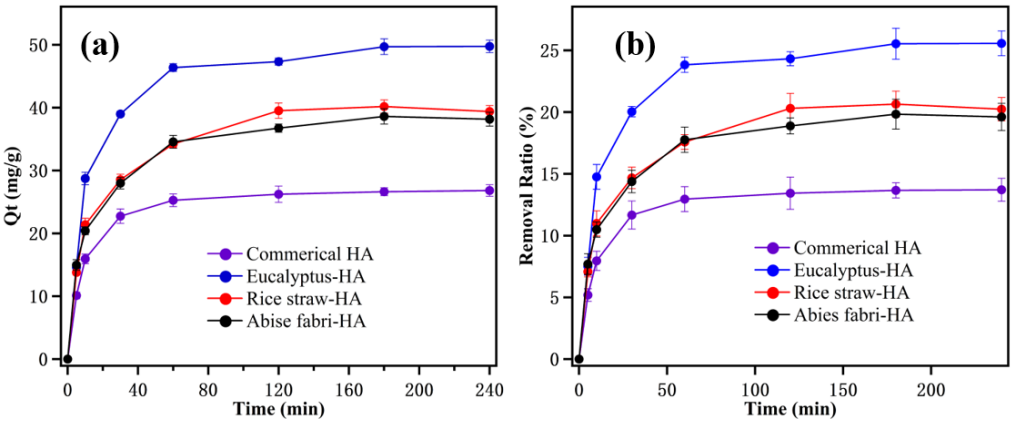


Figure 2. Comparison of Pb^{2+} adsorption capacities of humic acids from different sources: adsorption amount (**a**) and removal efficiency (**b**). The initial concentration of Pb^{2+} is 100 mg/L, with an initial solution pH of 5.0, a humic acid adsorbent mass of 0.1 g, and an adsorption temperature of 25 °C.

As shown in Figure 2a, both the hydrothermal humic acids synthesized from lignocellulosic biomass and the commercially purchased humic acids exhibit the ability to adsorb Pb^{2+}, with the adsorption amount increasing over time. Equilibrium was reached within 1 h for all humic acid adsorbents, indicating the potential of humic acids as effective Pb^{2+} removal agents. Notably, the Pb^{2+} adsorption performance varied among the humic acids from different sources under the same adsorption conditions. Commercial-HA exhibited the lowest Pb^{2+} adsorption capacity (26.82 mg/g) and removal efficiency (13.71%), while Eucalyptus-HA, representing broad-leaved humic acid, showed the highest Pb^{2+} adsorption capacity (49.75 mg/g) and removal efficiency (25.57%). The humic acids derived from softwood (Abise fabri) and grass biomass (rice straw) exhibited similar Pb^{2+} adsorption capacities (39.38 and 38.16 mg/g, respectively) and removal efficiencies (20.24% and 19.61%, respectively). These results suggest that the Pb^{2+} adsorption capacity of hydrothermal humic acids prepared from lignocellulosic biomass is influenced by the properties of the raw materials.

An elemental analysis of various humic acid samples and pore structures can be found in our previous published article [10]. The oxygen content varies significantly among humic acids from different sources, with Commercial-HA exhibiting the highest value at 52.64% and Rice straw-HA the lowest at 29.28%. Conversely, Rice straw-HA demonstrates the highest carbon content at 63.88%, while Commercial-HA shows the lowest at 41.4%. In general, the adsorption of heavy metal ions by humic acids primarily occurs through coordination, electrostatic interactions, adsorption, and ion exchange [12], which are also accompanied by redox reactions. For Pb^{2+}, factors such as the elemental composition, specific surface area, and heteroatom content of humic acids are key determinants of adsorption capacity. According to the specific surface area measurements of the humic acids presented in Section 3.1, Eucalyptus-HA exhibited the largest specific surface area (9.3134 m^2/g), the highest pore volume (0.042497 cm^3/g), and the largest pore size (18.04 nm), resulting in its superior Pb^{2+} adsorption performance. In contrast, Commercial-HA, with the lowest

specific surface area (0.7976 m^2/g), smallest pore volume (0.000927 cm^3/g), and smallest pore size (5.33 nm), demonstrated the poorest Pb^{2+} adsorption capacity.

However, despite Rice straw-HA having a relatively high specific surface area (6.7457 m^2/g), pore volume (0.020916 cm^3/g), and pore size (12.33 nm), it did not exhibit a particularly outstanding Pb^{2+} adsorption performance. This suggests that pore structure is not the sole factor influencing the adsorption of Pb^{2+} by humic acids. Combining this with the elemental analysis results (Table 1), it was found that Rice straw-HA had the lowest oxygen content (29.28 wt %), indicating that oxygen content is also an important factor affecting the performance of humic acids. Abies fabri-HA, on the other hand, exhibited superiority in neither pore structure nor oxygen content, which explains why its Pb^{2+} adsorption performance was comparable to that of Rice straw-HA.

Table 1. Elemental analysis of humic acid from different sources.

Samples	N (wt %)	C (wt %)	H (wt %)	S (wt %)	O (wt %)	H/C	O/C
Abise fabri-HA	0.06	59.44	5.46	1.02	34.02	1.10	0.43
Eucalyptus-HA	0.02	54.57	5.52	0.85	39.04	1.21	0.54
Rice straw-HA	0.53	63.88	5.64	0.67	29.28	1.06	0.34
Commercial-HA	0.75	41.40	4.09	1.12	52.64	1.19	0.95

Studies have also shown that heteroatoms such as nitrogen (N) can enhance the adsorption capacity for heavy metal ions through chelation, as lone pairs of electrons can form complexes with these ions [13]. However, as indicated by the nitrogen content in the elemental analysis of the lignocellulosic humic acids from different sources (Table 1), Commercial-HA had the highest N content, yet it did not demonstrate superior Pb^{2+} adsorption performance. This suggests that within the scope of this study, the chelation capacity of heteroatoms like N is not a primary factor influencing Pb^{2+} adsorption. In summary, pore structure is the most significant factor affecting the Pb^{2+} adsorption capacity of humic acids, having the greatest impact. Oxygen content is a secondary factor, while the content of heteroatoms such as N is of tertiary importance. For future research aimed at enhancing Pb^{2+} adsorption performance, it is recommended to prioritize the regulation of the pore structure of humic acids, optimizing for larger specific surface areas, pore volumes, and pore sizes. Additionally, efforts should be made to increase the oxygen content of the humic acids.

3.2. The Influence of Operational Parameters (Such as Initial Concentration and Solution pH) on Pb^{2+} Adsorption Capacity and the Recyclability of Humic Acid

The difference between the humic acid of eucalyptus powder and commercial humic acid in their adsorption properties of Pb^{2+} at different initial concentrations of Pb^{2+} and different initial pH values is shown in Figure 3, and the results of their removal rates are shown in Figure S2.

As the initial concentration of Pb^{2+} increased from 10 mg/L to 200 mg/L, the equilibrium adsorption capacity of commercial humic acid (Commercial-HA) for Pb^{2+} rose from 7.06 mg/g (removal efficiency of 35.38%) to 29.34 mg/g (removal efficiency of 7.54%). Similarly, the equilibrium adsorption capacity of Eucalyptus-HA increased from 8.99 mg/g (removal efficiency of 45.00%) to 47.50 mg/g (removal efficiency of 12.21%). At all initial concentrations, the Pb^{2+} adsorption performance of Eucalyptus-HA was superior to that of Commercial-HA, as discussed in Section 3.2, primarily due to the excellent specific surface area and pore structure of Eucalyptus-HA. Since the mass of humic acid added was constant, the number of adsorption sites was fixed. Therefore, at low initial concentrations of Pb^{2+}, the majority of the Pb^{2+} could be adsorbed. As the initial concentration of Pb^{2+}

increased, the concentration gradient between the Pb^{2+} in the aqueous phase and the ions on the humic acid surface also increased [9], resulting in higher equilibrium adsorption capacities. However, due to these excessive initial Pb^{2+} concentrations, the overall removal efficiency decreased.

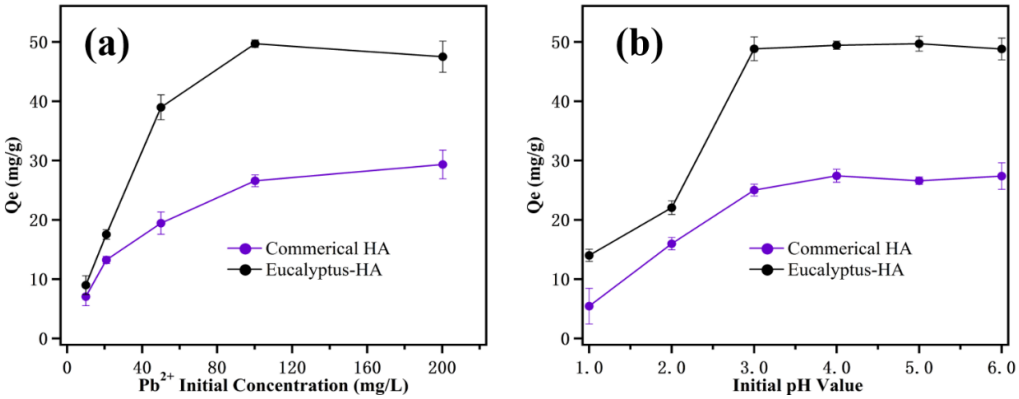


Figure 3. Effect of initial concentration (**a**) and pH (**b**) on equilibrium adsorption capacity of Pb^{2+} by Eucalyptus-HA and Commercial-HA. (**a**) The initial concentrations of Pb^{2+} were 10, 20, 50, 100, and 200 mg/L, the initial pH of the adsorbent was 5.0, the mass of the adsorbent humic acid was 0.1 g, the adsorption temperature was 25 °C, and the adsorption time was 180 min. (**b**) The initial concentration of Pb^{2+} was 100 mg/L, the mass of the adsorbent humic acid was 0.1 g, the adsorption temperature was 25 °C, and the adsorption time was 180 min.

The initial pH of the solution significantly affects Pb^{2+} adsorption, mainly by influencing the speciation of Pb and the competition between H^+ and Pb^{2+} for adsorption sites on the adsorbent surface [14]. When the solution pH is below 6, lead primarily exists as free Pb^{2+} ions. At pH values above 6, lead precipitates out of solutions by forming hydroxide complexes. Additionally, the humic acids synthesized in this study dissolve when the pH exceeds 6, limiting the pH range investigated in this study to 1–6. The equilibrium adsorption capacities of Pb^{2+} at different initial pH values are shown in Figure 3b. The results reveal that as pH increases, the equilibrium adsorption capacity of Pb^{2+} initially increases and then stabilizes. At lower pH values, the solution contains a high concentration of H^+ ions, which compete with positively charged Pb^{2+} for adsorption sites, reducing Pb^{2+} adsorption. Moreover, an excess of H^+ ions alters the surface charge of humic acids, further hindering Pb^{2+} adsorption [15]. Across the pH range studied, Eucalyptus-HA consistently outperformed Commercial-HA in Pb^{2+} adsorption. In addition to factors such as pore structure, the isoelectric point of Commercial-HA was 3.6, whereas Eucalyptus-HA had a slightly lower isoelectric point (2.4). This resulted in a greater negative surface charge at lower pH values, leading to stronger electrostatic interactions with positively charged Pb^{2+} ions and enhancing Pb^{2+} fixation on the surface.

The recycling performance of Eucalyptus-HA and Commercial-HA is illustrated in Figure 4. After each use, the humic acids were regenerated using a 1 M HNO_3 solution at room temperature.

The results indicate that both Commercial-HA and Eucalyptus-HA exhibit poor performance in repeated use. Commercial-HA's equilibrium adsorption capacity decreased from 26.58 mg/g (removal efficiency of 13.66%) after the first use to 8.79 mg/g (removal efficiency of 4.39%) after the fifth use. Similarly, Eucalyptus-HA's equilibrium adsorption capacity decreased from 49.69 mg/g (removal efficiency of 25.54%) after the first use to 22.99 mg/g (removal efficiency of 11.48%) after the fifth use.

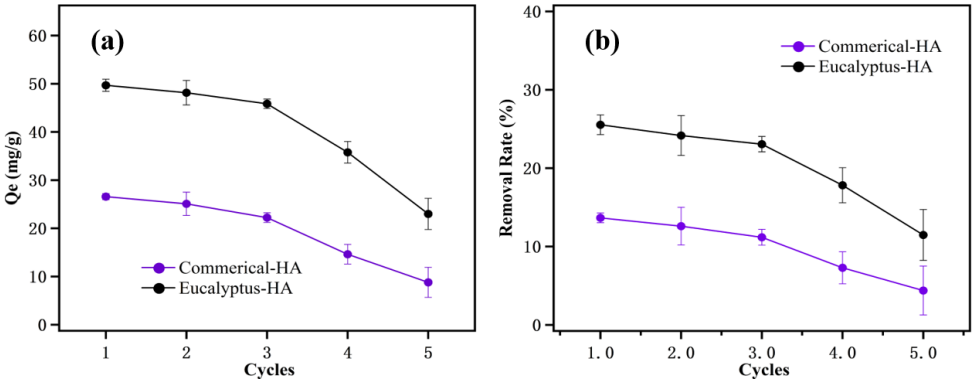


Figure 4. Repeated use of Eucalyptus-HA and Commercial-HA for Pb^{2+} adsorption: equilibrium adsorption capacity (**a**) and removal efficiency (**b**). Initial Pb^{2+} concentration was 100 mg/L, with an initial pH of 5.0, an adsorbent mass of 0.1 g, an adsorption temperature of 25 °C, and an adsorption duration of 180 min.

3.3. Comparative Study on Adsorption Behavior of Pb^{2+} Ions by Humic Acid

3.3.1. Adsorption Isotherms (Comparison of Langmuir and Freundlich Adsorption Models)

Adsorption isotherms provide a visual representation of the adsorption capacity of these samples in solutions containing lead ions at various concentrations. By applying different adsorption models, information such as the material's adsorption capacity and the type of adsorption mechanism can be obtained. Commercial-HA and Eucalyptus-HA were subjected to saturation adsorption experiments at various temperatures (25 °C, 35 °C, and 45 °C) and different initial Pb^{2+} concentrations (10, 20, 50, 100, and 200 mg/L). The equilibrium adsorption capacities (Q_e) and equilibrium concentrations at these temperatures are presented in Figure S3. The data were analyzed and fitted to different kinetic models, including the Langmuir adsorption model and the Freundlich model.

Langmuir adsorption model fitting formula:

$$\frac{C_e}{Q_e} = \frac{C_e}{Q_{maz}} + \frac{1}{Q_e \times K_L} \tag{4}$$

Freundlich model fitting formula:

$$lnQ_e = lnK_F + \frac{1}{n} \times lnC_e \tag{5}$$

In these equations, C_e and Q_e represent the equilibrium concentration of the solution and the corresponding maximum adsorption capacity at different initial Pb^{2+} concentrations. Q_{maz} denotes the maximum adsorption capacity of Pb^{2+} at a given temperature. K_L is the Langmuir adsorption equilibrium constant, K_F is the Freundlich isotherm constant, and n is the adsorption intensity constant that characterizes the adsorption capacity. Additionally, the Langmuir adsorption model defines a dimensionless separation factor R_L as follows:

$$R_L = \frac{1}{1 + C_0 \times K_L} \tag{6}$$

The fitting results of the different adsorption models are shown in Figure 5. The model parameters Q_{maz}, K_L, n, and K_F, along with the corresponding correlation coefficients, R^2, for each fitting model are summarized in Table 2. Based on the fitting results of the different models at various initial Pb^{2+} concentrations, the values of K_F and R_L for Eucalyptus-HA and Commercial-HA during Pb^{2+} adsorption are presented in Tables S1 and S2, respectively.

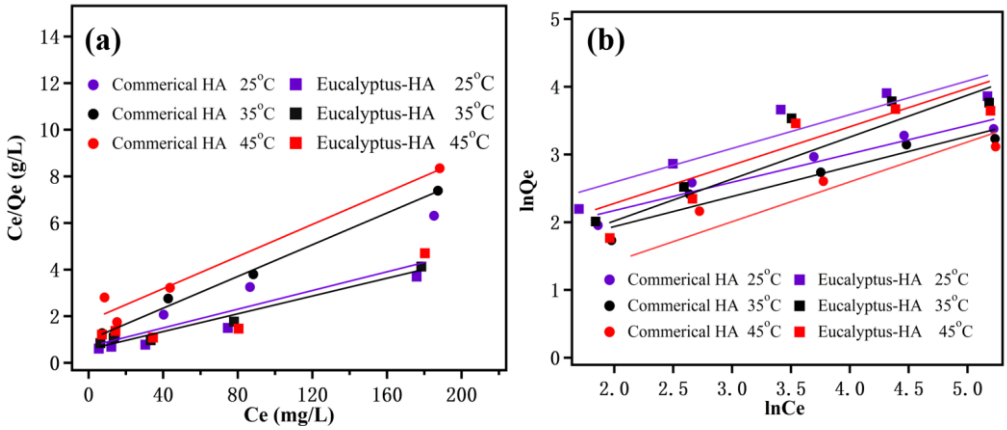


Figure 5. Adsorption isotherm fitting for Pb^{2+} by Eucalyptus-HA and Commercial-HA: (**a**) Langmuir adsorption model fitting and (**b**) Freundlich adsorption model fitting. Initial Pb^{2+} concentrations were 10, 20, 50, 100, and 200 mg/L, with an initial solution pH of 5.0, a humic acid mass of 0.1 g, and an adsorption duration of 180 min.

Table 2. Fitting results of different adsorption isotherm models for Pb^{2+} adsorption onto humic acid.

Adsorption Isotherm Model	Parameters	Commercial-HA			Eucalyptus-HA		
		298.15 K	308.15 K	318.15 K	298.15 K	308.15 K	318.15 K
Langmuir	Qmax (mg/g)	33.1708	29.38325	29.03348	54.36850976	52.43288591	49.8678502
	K_L (L/mg)	0.041921	0.03458	0.019051	0.05124112	0.033011389	0.028702498
	R^2	0.9993	0.996286	0.983781	0.9913	0.983556	0.931892
Freundlich	n	2.392974	2.254385	1.699322	2.00775	1.768003	1.615457
	K_F	3.808746	2.853939	1.274419	4.930301	3.147159	2.183218
	R^2	0.97094	0.963437	0.922775	0.925579	0.934531	0.922797

According to Table 2, the linear correlation coefficients R^2 obtained from fitting the Langmuir adsorption model for both Eucalyptus-HA and Commercial-HA were superior to those from the Freundlich model, indicating that the adsorption of Pb^{2+} by Eucalyptus-HA and Commercial-HA more closely follows the Langmuir monolayer adsorption model. This finding is consistent with the results reported in the reference [8]. At different temperatures, Eucalyptus-HA consistently demonstrated a better Pb^{2+} adsorption capacity compared to Commercial-HA. The maximum theoretical Pb^{2+} adsorption capacities for Eucalyptus-HA were 33.17 mg/g (25 °C), 29.38 mg/g (35 °C), and 29.03 mg/g (45 °C). For Commercial-HA, these values were 54.37 mg/g (25 °C), 52.43 mg/g (35 °C), and 49.87 mg/g (45 °C). The reference [8] reported that the maximum Pb^{2+} adsorption capacities for sludge-derived humic acid, using the Langmuir model, were 27.59 mg/g (25 °C), 24.74 mg/g (35 °C), and 23.57 mg/g (45 °C). Another reference [16] found that the maximum Pb^{2+} adsorption capacities for lignite-derived humic acid were 146.94 mg/g (25 °C), 144.33 mg/g (35 °C), and 136.86 mg/g (45 °C). The observed differences in Pb^{2+} adsorption capacities among various humic acids are attributed to the distinct sources of the humic acids, which result in variations in raw material composition. Additionally, differences in the methods of humic acid extraction led to variations in the resulting microstructures of the humic acids.

The dimensionless separation factor R_L can be used to evaluate the feasibility of adsorption reactions [17,18]. When R_L equals 1, the adsorption is linear; when R_L is greater than 1, the conditions are unfavorable for adsorption; and when R_L is between 0 and 1, the conditions are favorable for adsorption [19]. According to Tables S2 and S3, the R_L values for Eucalyptus-HA and Commercial-HA during Pb^{2+} adsorption at different temperatures and initial Pb^{2+} concentrations are all within the range of 0 to 1. This indicates that the

adsorption conditions are favorable for Pb^{2+} removal and that the adsorption process is spontaneous.

The Freundlich isotherm parameter n can be used to characterize the adsorption intensity [20]. When $n < 1$, the adsorption process is difficult to carry out under the condition; when $1 < n < 2$, adsorption is moderately difficult; and when $n > 2$, adsorption is highly favorable [21]. According to the results in Table 2, as the temperature increases, the n values for both Eucalyptus-HA and Commercial-HA decrease, indicating that higher temperatures are less favorable for Pb^{2+} adsorption. Commercial-HA exhibited higher n values compared to Eucalyptus-HA, suggesting that Pb^{2+} is more readily adsorbed onto Commercial-HA. However, due to its lower specific surface area, the maximum Pb^{2+} adsorption capacity of Commercial-HA remains relatively low.

3.3.2. Adsorption Kinetics and Thermodynamics of Pb^{2+} by Humic Acid

To better understand the adsorption process and mechanism of Pb^{2+} on the surface of humic acid, the quasi-first-order and quasi-second-order kinetic models were employed to describe and analyze the adsorption process in solution. Under the condition of an initial Pb^{2+} concentration of 100 mg/L, the changes in Pb^{2+} concentration over time at different temperatures are shown in Figures S3 and S4. The results indicate that an increase in temperature is unfavorable for the adsorption of Pb^{2+} by different humic acids. Although higher temperatures can enhance the diffusion rate of Pb^{2+}, the increased thermal motion of Pb^{2+} molecules weakens the adsorption capacity [22].

Quasi-first-order kinetic model [23]:

$$\ln(Q_e - Q_t) = \ln Q_m - k_1 * t \tag{7}$$

Quasi-second-order kinetic model:

$$\frac{t}{Q_t} = \frac{1}{k_2 * {Q_e}^2} + \frac{t}{Q_e} \tag{8}$$

In the above equations, Q_e represents the equilibrium adsorption capacity of Pb^{2+} at a given temperature (mg/g), Q_m is the maximum adsorption capacity, t is the adsorption time, and k_1 and k_2 are the adsorption rate constants for the respective models. The fitting results are shown in Figure 6, and the derived kinetic parameters are listed in Table S3.

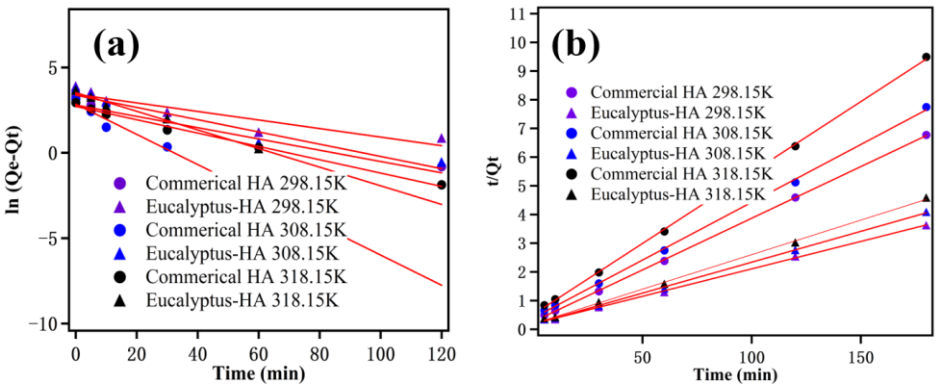


Figure 6. The fitting of quasi-first-order and quasi-second-order kinetic models for Pb^{2+} adsorption onto Eucalyptus-HA and Commercial-HA. The initial Pb^{2+} concentration was 100 mg/L, with an initial solution pH of 5.0 and 0.1 g of humic acid used as the adsorbent. (**a**) Fitting of quasi-first-order kinetic model and (**b**) fitting of quasi-second-order kinetic model.

According to the results in Table S4, the correlation coefficients for the quasi-second-order kinetic model were higher than those for the quasi-first-order model at different

temperatures for both Commercial-HA and Eucalyptus-HA. Additionally, the maximum adsorption capacity obtained from the quasi-second-order model closely matches the experimental values, indicating that the adsorption process for the different humic acid samples is more consistent with the second-order kinetic model, which aligns with the findings in the literature. The adsorption rate constant k_2 and the equilibrium adsorption capacity Q_e derived from the quasi-second-order model suggest that Commercial-HA exhibits a faster adsorption rate for Pb^{2+}. This is consistent with the results from the adsorption isotherms discussed in Section 3.3.1.

Based on the rate constant k_2 obtained from the quasi-second-order kinetic model at different temperatures, the Arrhenius equation [24] was used to calculate the pre-exponential factor A and activation energy E_a for both Commercial-HA and Eucalyptus-HA. Using the following equations, the enthalpy change ΔH, entropy change ΔS, and ΔG for the adsorption process of Pb^{2+} onto the humic acids were further fitted [25]. The fitting results are shown in Figure S5, and the fitted data are presented in Table 3.

$$ln\frac{Q_e}{C_e} = -\frac{\Delta H}{RT} + \frac{\Delta S}{R} \tag{9}$$

$$\Delta G = \Delta H - T \times \Delta S \tag{10}$$

Table 3. Thermodynamic parameters of Pb^{2+} adsorption process of Commercial-HA and Eucalyptus-HA.

Commercial-HA						
A	E_a (KJ/mol)	ΔH (J/mol)	ΔS (J/mol × K)	ΔG (J/mol)		
				298.15 (K)	308.15 (K)	318.15 (K)
1.15098	36.41865	−15,086	60.29729	−33,064	−33,667	−34,270
Eucalyptus-HA						
A	Ea (KJ/mol)	ΔH (J/mol)	ΔS (J/mol × K)	ΔG (J/mol)		
				298.15 (K)	308.15 (K)	318.15 (K)
1.000751	1.690319	−12,266.5	44.53062	−25,543.3	−25,988.6	−26,433.9

Interestingly, based on the activation energy results, Commercial-HA exhibited a higher activation energy, indicating that from a thermodynamic perspective, there was a certain resistance to Pb^{2+} adsorption. However, previous kinetic studies have shown that Commercial-HA has a larger rate constant k_2. This analysis highlights that both thermodynamics and kinetics play important roles in the Pb^{2+} adsorption process, and the overall mechanism is relatively complex. For both Commercial-HA and Eucalyptus-HA, ΔH and ΔG were found to be negative, indicating that the adsorption process is exothermic and spontaneous. The ΔG values for Eucalyptus-HA were consistently smaller than those for Commercial-HA, suggesting that the tendency for spontaneous Pb^{2+} adsorption is stronger for Commercial-HA, aligning with the adsorption isotherms in Section 3.3.1 and the prior kinetic results. Additionally, as the temperature increased, the absolute value of ΔG slightly increased, suggesting that from a thermodynamic perspective, elevated temperatures are unfavorable for the adsorption process.

In summary, a comparative analysis of the adsorption kinetics and thermodynamics of Pb^{2+} onto Commercial-HA and Eucalyptus-HA revealed that Commercial-HA exhibits a faster Pb^{2+} adsorption rate. However, due to thermodynamic limitations and its relatively low specific surface area, the adsorption capacity for Pb^{2+} was not very high. Future research could focus on further enhancing the three-dimensional structure of humic acid to provide more active sites for Pb^{2+} ion adsorption.

3.4. Comparative Study on Humic Acid Diffusion Model of Pb^{2+}

The quasi-second-order kinetic model can effectively reflect the adsorption rate of Pb^{2+} onto humic acid; however, it cannot describe the diffusion of Pb^{2+} from the bulk solution to the surface of the humic acid. In this section, the intraparticle diffusion model will be applied to further investigate the adsorption of Pb^{2+} onto Commercial-HA and Eucalyptus-HA. The fitting equation is shown as follows [26].

$$Q_t = C + k_p * t^{1/2} \tag{11}$$

In this equation, k_p represents the intraparticle diffusion model parameter ($mg \cdot g^{-1} \cdot min^{1/2}$), and C is the boundary layer constant ($mg \cdot g^{-1}$). The fitting results of the intraparticle diffusion model for Pb^{2+} adsorption onto Commercial-HA and Eucalyptus-HA at different temperatures are shown in Figure 7, and the fitted data can be found in Table S4.

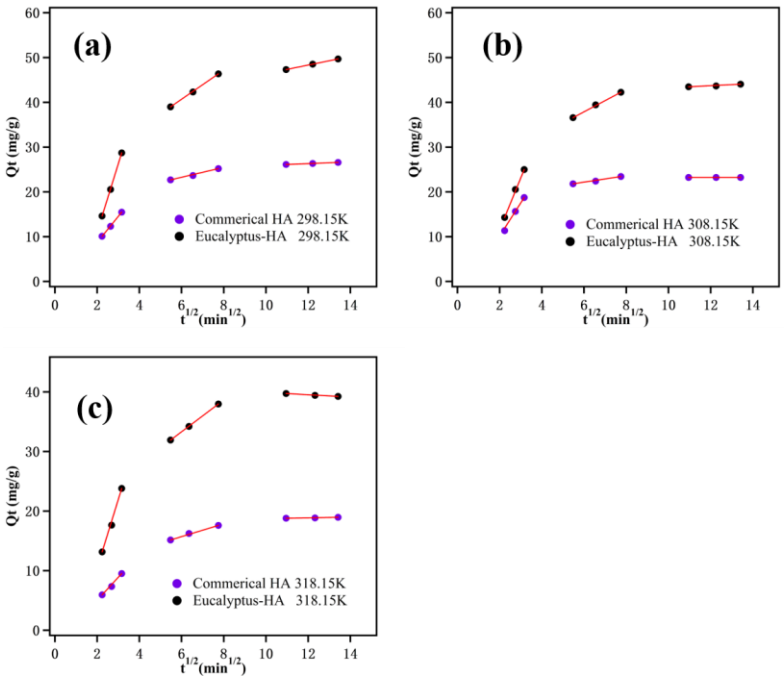


Figure 7. Intraparticle diffusion model of Pb^{2+} adsorbed onto Commercial-HA and Eucalyptus-HA at different temperatures: (**a**) 298.15 K, (**b**) 308.15 K, and (**c**) 318.15 K.

The adsorption process of Commercial-HA and Eucalyptus-HA at different temperatures can be divided into three stages: the external mass transfer stage (0–20 min), the internal mass transfer stage (20–60 min), and the equilibrium adsorption stage (60–180 min). According to the results in Table S4, the relationships $k_1 > k_2 > k_3$ and $C_1 < C_2 < C_3$ indicate that the liquid film diffusion process is rapid [26]. In the initial adsorption phase, there are abundant available sites on the surface of the humic acid, making external diffusion the primary factor influencing adsorption. Subsequently, once the surface of the humic acid becomes saturated, internal diffusion plays a dominant role. The adsorption rate decreases due to the mass transfer resistance within the internal pores of the humic acid, ultimately reaching adsorption equilibrium. Moreover, Eucalyptus-HA demonstrates a higher diffusion rate at each stage compared to Commercial-HA, indicating that both internal and external diffusion resistances are lower for Eucalyptus-HA, facilitating a more efficient adsorption of Pb^{2+}.

The sources of raw materials for the preparation of humic acid through hydrothermal reaction are extensive, particularly comprising agricultural wastes (such as rice straw and wheat straw) and other lignocellulosic biomass resources, which provide a raw material

foundation for its large-scale preparation. Through a pretreatment of the raw materials (such as alkali treatment, etc.), the yield of humic acid prepared through hydrothermal reaction can be effectively enhanced and the production cost can be reduced. Additionally, the physicochemical properties of humic acid (such as specific surface area and types of functional groups) can be further optimized through a pretreatment of the raw materials (such as the introduction of more carboxyl or phenolic hydroxyl groups) to meet the adsorption requirements of different heavy metals or pollutants.

In contrast to traditional methods for removing Pb^{2+} (such as chemical precipitation, ion exchange, activated carbon adsorption, etc.), the major advantage of humic acid derived from hydrothermal reaction lies in the low cost and wide availability of raw materials. Taking agricultural wastes as an example, the cost of these by-products is almost negligible, and the cost of converting them into humic acid through hydrothermal reaction is much lower than that of activated carbon production or resin synthesis. Furthermore, as a natural material, humic acid is environmentally friendly and renewable. The residues generated during its preparation can also be utilized for other purposes (such as soil amendments), further reducing the cost of waste treatment.

The pore structure of humic acid is the primary factor influencing its adsorption capacity for Pb^{2+}, followed by the content of oxygen (O) elements, and then the content of nitrogen (N) and other heteroatoms. Eucalyptus-derived humic acid (Eucalyptus-HA) exhibits a lower point of zero charge. The initial concentration of Pb^{2+} and the pH of the solution have significant effects on the Pb^{2+} adsorption capacity of humic acid. With a limited addition of humic acid, an excessively high initial Pb^{2+} concentration increases the saturation adsorption amount but decreases the removal rate; conversely, an excessively low pH reduces the removal rate due to competitive adsorption between H^+ and Pb^{2+}. Due to the instability of their pore structures, both types of humic acid demonstrate poor reusability.

The fitting results of the adsorption isotherms indicate that the adsorption of Pb^{2+} by both types of humic acid aligns more closely with the Langmuir model. Commercial humic acid performs better in terms of its adsorption rate but is limited by thermodynamics and its relatively poor specific surface area, resulting in a lower adsorption capacity. The fitting results of the intraparticle diffusion model reveal that the liquid film diffusion process of Pb^{2+} is rapid, and Eucalyptus-HA exhibits higher diffusion rates than commercial humic acid at all stages. This suggests that Eucalyptus-HA has smaller intraparticle and external diffusion resistances, making it more prone to Pb^{2+} adsorption. Therefore, enhancing the specific surface area, pore structure, and stability of humic acid is a crucial approach to improving its heavy metal adsorption and reusability. This study provides a method for preparing humic acids with different structures and Pb^{2+} adsorption capabilities from lignocellulosic biomass sources and offers a reference for the targeted regulation of humic acid structure and composition in various application scenarios.

4. Conclusions

Eucalyptus-HA exhibits a superior adsorption capacity and removal efficiency for Pb^{2+} compared to Commercial-HA. Specifically, at an initial Pb^{2+} concentration of 100 mg/L, Eucalyptus-HA achieves an adsorption capacity of 49.75 mg/g and a removal efficiency of 25.57%, whereas Commercial-HA demonstrates significantly lower values of 26.82 mg/g and 13.71%, respectively. The adsorption performance of Eucalyptus-HA surpasses that of Commercial-HA across various initial concentrations and pH levels of Pb^{2+}. Additionally, the initial concentration of Pb^{2+} and the pH of the solution significantly influence the adsorption capacity of humic acid towards Pb^{2+}. In scenarios with limited humic acid addition, a higher initial Pb^{2+} concentration enhances saturated adsorption but reduces

removal efficiency. An excessively low pH leads to competitive adsorption between H^+ ions and Pb^{2+}, thereby diminishing the removal rate of Pb^{2+}. Due to the instability of humic acid pores, both Commercial-HA and Eucalyptus-HA exhibit poor reusability.

The fitting results of the adsorption isotherm indicate that the adsorption of Pb^{2+} by both Commercial-HA and Eucalyptus-HA aligns most closely with the Langmuir model. Despite this, Commercial-HA shows a better adsorption rate, which is constrained by its thermodynamic limitations and inferior specific surface area, resulting in a poorer adsorption capacity for Pb^{2+}.

The intraparticle diffusion model further elucidates the Pb^{2+} adsorption process of Commercial-HA and Eucalyptus-HA. The results demonstrate that the liquid film diffusion of Pb^{2+} occurs relatively rapidly at different temperatures. Moreover, Eucalyptus-HA exhibits higher diffusion rates than Commercial-HA at various stages, indicating lower internal and external diffusion resistance, thus facilitating Pb^{2+} adsorption.

These findings suggest that enhancing the specific surface area and pore structure stability of humic acid is crucial for improving its adsorption and removal of heavy metals, as well as its reusability. This study provides insights into the preparation of humic acids with distinct structural and behavioral characteristics towards Pb^{2+} from a wood fiber source perspective, offering valuable references for the targeted regulation of humic acid structure and composition in diverse application scenarios.

Supplementary Materials: The following supporting information can be downloaded at https://www.mdpi.com/article/10.3390/pr13010155/s1, Figure S1: Effects of initial Pb^{2+} concentration (a) and pH (b) on the removal efficiency of Eucalyptus-HA and Commercial-HA. (a) The initial Pb^{2+} concentrations are 10, 20, 50, 100, and 200 mg/L, with an initial solution pH of 5.0, 0.1 g of humic acid adsorbent, an adsorption temperature of 25 °C, and an adsorption time of 180 min. (b) The initial Pb^{2+} concentration is 100 mg/L, with 0.1 g of humic acid adsorbent, an adsorption temperature of 25 °C, and an adsorption time of 180 min. Figure S2: Relationship between equilibrium adsorption capacity and equilibrium concentration of Pb^{2+} for Eucalyptus-HA and Commercial-HA at different temperatures and initial Pb^{2+} concentrations. The initial Pb^{2+} concentrations are 10, 20, 50, 100, and 200 mg/L, with an initial solution pH of 5.0, a solution volume of 200 mL, 0.1 g of humic acid adsorbent, and an adsorption time of 180 min. Figure S3: Relationship between Pb^{2+} concentration and time for Commercial-HA and Eucalyptus-HA at different temperatures and durations. The initial Pb^{2+} concentration is 100 mg/L, with an initial solution pH of 5.0 and 0.1 g of humic acid adsorbent. Figure S4: Adsorption capacity of Pb^{2+} onto Commercial-HA and Eucalyptus-HA over time at different temperatures. The initial Pb^{2+} concentration is 100 mg/L, with an initial solution pH of 5.0 and 0.1 g of humic acid adsorbent. Figure S5: Fitted thermodynamic parameters for the adsorption process of Pb^{2+} onto Commercial-HA and Eucalyptus-HA. Table S1: KL and RL fitting results for Commercial-HA at different temperatures and initial Pb^{2+} concentrations. Table S2: KL and RL fitting results for Eucalyptus-HA at different temperatures and initial Pb^{2+} concentrations. Table S3: Fitted kinetic model parameters for Commercial-HA and Eucalyptus-HA. Table S4: Summary of intraparticle diffusion model parameters for Pb^{2+} adsorption onto humic acid at different temperatures.

Author Contributions: Conceptualization, C.S.; methodology, C.S.; software, J.L.; validation, J.L., L.Z., and J.W.; formal analysis, J.W.; investigation, L.Z.; resources, X.S.; data curation, C.S.; writing—original draft preparation, C.S.; writing—review and editing, J.W.; visualization, L.Z.; supervision, L.Z.; project administration, L.Z.; funding acquisition, L.Z. All authors have read and agreed to the published version of the manuscript.

Funding: This work was sponsored by the National Natural Science Foundation of China (22368051), Projects of Talents Recruitment of GDUPT (2023rcyj2005).

Data Availability Statement: The data are contained within the article.

Conflicts of Interest: The authors declare no conflicts of interest.

References

1. Yang, F.; Antonietti, M. Artificial Humic Acids: Sustainable Materials against Climate Change. *Adv. Sci.* **2020**, *7*, 1902992. [CrossRef]
2. Forotaghe, Z.A.; Souri, M.K.; Jahromi, M.G.; Torkashvand, A.M. Influence of Humic Acid Application on Onion Growth Characteristics under Water Deficit Conditions. *J. Plant Nutr.* **2022**, *45*, 1030–1040. [CrossRef]
3. Ampong, K.; Thilakaranthna, M.S.; Gorim, L.Y. Understanding the Role of Humic Acids on Crop Performance and Soil Health. *Front. Agron.* **2022**, *4*, 848621. [CrossRef]
4. Zhu, X.; Liu, J.; Li, L.; Zhen, G.; Lu, X.; Zhang, J.; Liu, H.; Zhou, Z.; Wu, Z.; Zhang, X. Prospects for Humic Acids Treatment and Recovery in Wastewater: A Review. *Chemosphere* **2023**, *312*, 137193. [CrossRef] [PubMed]
5. Yang, F.; Zhang, S.; Cheng, K.; Antonietti, M. A Hydrothermal Process to Turn Waste Biomass into Artificial Fulvic and Humic Acids for Soil Remediation. *Sci. Total Environ.* **2019**, *686*, 1140–1151. [CrossRef]
6. Chen, P.; Yang, R.; Pei, Y.; Yang, Y.; Cheng, J.; He, D.; Huang, Q.; Zhong, H.; Jin, F. Hydrothermal Synthesis of Similar Mineral-Sourced Humic Acid from Food Waste and the Role of Protein. *Sci. Total Environ.* **2022**, *828*, 154440. [CrossRef] [PubMed]
7. Song, C.; Zhang, L.; Wang, J.; Yu, X.; Xiao, Y.; Cheng, L.; Shu, X. Lignocellulose Hydrothermal Artificial Humic Acid Production: Reaction Parameters Screening and Investigation of Model/Real Feedstock. *J. Anal. Appl. Pyrolysis* **2024**, *183*, 106739. [CrossRef]
8. Dai, L.; Zhao, W.; Wei, B.; Zhang, K.; Han, T. Adsorption of Pb2+ by Insolubilized Humic Acid Extracted from Sewage Sludge. *J. Mater. Cycles Waste Manag.* **2021**, *23*, 1037–1047. [CrossRef]
9. Zhao, P.; Huang, Z.; Ma, Q.; Zhang, B.; Wang, P. Artificial Humic Acid Synthesized from Food Wastes: An Efficient and Recyclable Adsorbent of Pb (II) and Cd (II) from Aqueous Solution. *Environ. Technol. Innov.* **2022**, *27*, 102399. [CrossRef]
10. Liu, X.; Yang, H.; Li, G.; Ye, C.; Jin, H.; Tang, Y. Kinetics, Mechanisms and Release of Nitrogen-Containing Components during Pyrolysis of Chlorella with Potassium Hydroxide Addition. *J. Anal. Appl. Pyrolysis* **2024**, *183*, 106766. [CrossRef]
11. Takács, A.; Napolitano, R.; Purgel, M.; Bényei, A.C.; Zékány, L.; Brücher, E.; Tóth, I.; Baranyai, Z.; Aime, S. Solution Structures, Stabilities, Kinetics, and Dynamics of DO3A and DO3A–Sulphonamide Complexes. *Inorg. Chem.* **2014**, *53*, 2858–2872. [CrossRef] [PubMed]
12. Wang, J.; Li, H.; Yue, D. Enhanced Adsorption of Humic/Fulvic Acids onto Urea-Derived Graphitic Carbon Nitride. *J. Hazard. Mater.* **2022**, *424*, 127643. [CrossRef] [PubMed]
13. Pramanik, S.; Pathak, S.; Frontera, A.; Mukhopadhyay, S. Exploration of Supramolecular and Theoretical Aspects of Two New Cu(II) Complexes: On the Importance of Lone Pair···π(Chelate Ring) and Π···π(Chelate Ring) Interactions. *J. Mol. Struct.* **2022**, *1265*, 133358. [CrossRef]
14. Wang, Y.; Huang, Z.; Sheng, L.; Ma, Y. Effect of Modified Humic Acid Residue on the Adsorption and Passivation of Hg2+/Pb2+ in Solution and Soil. *J. Mol. Liq.* **2023**, *377*, 121581. [CrossRef]
15. Lin, D.; Tian, X.; Li, T.; Zhang, Z.; He, X.; Xing, B. Surface-Bound Humic Acid Increased Pb2+ Sorption on Carbon Nanotubes. *Environ. Pollut.* **2012**, *167*, 138–147. [CrossRef] [PubMed]
16. Meng, F.; Zhang, Y.; Cai, Y.; Yuan, G.; Feng, X. Han Kinetic and Thermodynamic Features of Pb (II) Removal from Aqueous Solution by Leonardite-Derived Humic Acid. *Water Air Soil Pollut.* **2021**, *232*, 255. [CrossRef]
17. Samaraweera, H.; Sharp, A.; Edwards, J.; Pittman, C.U.; Zhang, X.; Hassan, E.B.; Thirumalai, R.V.K.G.; Warren, S.; Reid, C.; Mlsna, T. Lignite, Thermally-Modified and Ca/Mg-Modified Lignite for Phosphate Remediation. *Sci. Total Environ.* **2021**, *773*, 145631. [CrossRef] [PubMed]
18. Babakhani, A.; Sartaj, M. Competitive Adsorption of Nickel(II) and Cadmium(II) Ions by Chitosan Cross-Linked with Sodium Tripolyphosphate. *Chem. Eng. Commun.* **2022**, *209*, 1348–1366. [CrossRef]
19. Li, J.; Huang, Q.; Yu, H.; Yan, L. Enhanced Removal Performance and Mechanistic Study of Cu2+, Cd2+, and Pb2+ by Magnetic Layered Double Hydroxide Nanosheets Assembled on Graphene Oxide. *J. Water Process Eng.* **2022**, *48*, 102893. [CrossRef]
20. Peruchi, L.M.; Fostier, A.H.; Rath, S. Sorption of Norfloxacin in Soils: Analytical Method, Kinetics and Freundlich Isotherms. *Chemosphere* **2015**, *119*, 310–317. [CrossRef] [PubMed]
21. Alkas, T.R.; Purnomo, A.S.; Pratiwi, A.N.; Nurwijayanti, Y.; Ediati, R.; Ersam, T.; Kusumawati, Y. Immobilization of UiO-66/Brown-Rot Fungi (BRF) in PVA-SA Matrix and Its Performance for Methylene Blue Decolorization. *Mater. Today Chem.* **2023**, *29*, 101411. [CrossRef]
22. Xu, Z.; Hu, Y.; Guo, Z.; Xiao, X.; Peng, C.; Zeng, P. Optimizing Pyrolysis Temperature of Contaminated Rice Straw Biochar: Heavy Metal(Loid) Deportment, Properties Evolution, and Pb Adsorption/Immobilization. *J. Saudi Chem. Soc.* **2022**, *26*, 101439. [CrossRef]
23. Du, Q.; Li, G.; Zhang, S.; Song, J.; Zhao, Y.; Yang, F. High-Dispersion Zero-Valent Iron Particles Stabilized by Artificial Humic Acid for Lead Ion Removal. *J. Hazard. Mater.* **2020**, *383*, 121170. [CrossRef] [PubMed]

24. Alarcón, E.A.; Villa, A.L. Curvature Arrhenius Plot for Estimation of Arrhenius Parameters and Adsorption Enthalpies for a Dual-Site (Bimolecular) Reaction. *Chem. Eng. Sci.* **2022**, *260*, 117879. [CrossRef]
25. Somer, T.D.; Roosen, M.; Harinck, L.; Geem, K.M.V.; Meester, S.D. Removal of Volatile Components from Plastic Waste in Liquid Media: Effect of Temperature and Particle Size. *Resour. Conserv. Recycl.* **2022**, *182*, 106267. [CrossRef]
26. Fan, X.; Wang, X.; Cai, Y.; Xie, H.; Han, S.; Hao, C. Functionalized Cotton Charcoal/Chitosan Biomass-Based Hydrogel for Capturing Pb2+, Cu2+ and MB. *J. Hazard. Mater.* **2022**, *423*, 127191. [CrossRef] [PubMed]

Disclaimer/Publisher's Note: The statements, opinions and data contained in all publications are solely those of the individual author(s) and contributor(s) and not of MDPI and/or the editor(s). MDPI and/or the editor(s) disclaim responsibility for any injury to people or property resulting from any ideas, methods, instructions or products referred to in the content.